https://doi.org/10.48048/tis.2022.4584

Two-Dimensional Finite Element Method for Modeling Edge Effects in Cross-Ply Laminates

Karim Sweilem Numayr and Hashem Khaled Almashaqbeh*

Department of Civil Engineering, Isra University, Amman 11622, Jordan

(*Corresponding author's e-mail: h.almashaqbeh@iu.edu.jo)

Received: 9 March 2021, Revised: 6 June 2021, Accepted: 6 July 2021

Abstract

A 2-dimensional finite element (FE) method, based on an approximate analytical solution, is developed to define accurately stress fields and boundary layer width in symmetrically laminated composites. A better insight into the edge effect and delamination failure of cross-ply laminates is attained through a physical explanation of the mathematical FE solution. While some other solutions failed, the present FE solution obtains accurate results using a limited number of elements, and therefore reduces computer storage and computation time. A perturbation technique is employed to derive shape functions for the free edge boundary region, which properly describes the physics of sudden exponential growth of stress field in the vicinity of the edge. An original and comprehensive FE computer program is developed, using these specific shape functions, special numerical integration, and mesh generation algorithms. Results for bidirectional laminates under uniaxial extension are presented and compared with finite difference, FE, and approximate analytical solution.

Keywords: Finite element modeling and programing, Exponential shape functions, Cross-ply laminates, Edge effect, Delamination

Introduction

Due to the wide use of composite materials, it is important that engineers have a good insight into the free edge effects in composite laminates. From previous experimental, numerical, and approximate analytical solutions, it is known that composite laminates develop interlaminar stress concentrations near the free edge region [1]. Characterizing and understanding of the various failure modes, which have been demonstrated in composite laminates, depends on an accurate determination of the stress field in the free edge region [2]. The boundary layer effect is believed to play a major role in initiating the delamination failure in some laminates. Therefore, this effect is important in determining the strength of such laminates. However, there exist major deficiencies in the ability of most theories to determine the stress field in regions of stress concentration, where classical lamination theory does not yield accurate results, [1,3,4]. Several authors have investigated the free-edge effect in symmetrically laminated composite plates under uniform one-dimensional stretch. They have used different approaches in their analysis; some used experimental procedures [5-9] and others used analytical analysis, in order to define the stress distribution. Some have succeeded in establishing approximate analytical solutions using the perturbation technique [10], and some have used numerical procedures such as the finite difference method [11-13] and the FE [1,2,14-23] method. On the other hand, some researchers have used the geometric potential theory to explain the edge effect [24-28]. Pipes and Pagano [11] have developed an analytical solution, based on a linear elastic generalized plane strain formulation, using a finite difference procedure. They have shown that certain interlaminar stresses will rise in magnitude near the free-edge boundary region. Since a coarse gridwork was used to reduce computer storage and computing time, their results were not detailed enough to allow the accurate evaluation of stresses near the free-edge region. Pagano [13] has proposed a theory to define the complete stress field within an arbitrary composite laminate. His theory is based upon an extension of Reissner's variation theorem as a mechanism to develop the appropriate field equations in composite laminates. His work provides good results for composite laminates with few layers. However, difficulties are encountered in using the method to realistically define the stress fields in laminates consisting of many layers. The Perturbation technique was used by Tang [29] to establish an

approximate solution to certain 4^{th}-order partial differential equations which are expressed in terms of stress functions. These 4^{th}-order partial differential equations resulted from the satisfaction of displacement compatibility equations. Hsu and Herakovich [9] employed a 0^{th}-order perturbation approximation in terms of displacement function along with a limiting free body approach in order to establish a solution to the governing system of partial differential equations. This solution depends on the geometric thickness to width ratio L_3/L_2; the smaller this ratio, the more accurate is the solution. The solution predicts a continuous distribution of interlaminar stresses with maximum values in the free-edge boundary region. Wang and Dickson [30] represented the interlaminar stresses and displacements of each layer in terms of a series of Legendre polynomials. The extended Galerkin method was used to satisfy the equilibrium equations for each layer. The results of this investigation predict high normal stress at the free edges. The FE method is widely used in the design of practical composite structural elements. Isakson and Levy [14] modeled a symmetrical laminate of finite width using a set of anisotropic layers separated by isotropic shear layers. The peel stress was assumed to be 0 and other stresses are calculated using the constant strain assumption within each element. Stanton *et al.* [15] used a tri-cube isoparametric discrete element and a system to automate the construction of the FE model. In their large element formulation, the data input requirements are reduced considerably. Wang and Crossman [16] investigated symmetrically laminated plates. They employed triangular finite elements to investigate the stress field closest to the ply interfaces and the free edges of the laminate. They used a simplified method [17] to estimate the interlaminar stresses in composite laminates. The method is based on a smearing technique in which 2 or more laminas are considered as one quasi-homogeneous lamina. Bar-Yoseph and Avrashi [18] used a modified mixed-hybrid finite element to solve the edge layer problem in composite laminates. They carried out a 3-dimensional stress analysis, in which the method of composite expansions along with Hellinger - Reissner variation formulation was used. Barboni *et al.* [19] investigated the 3-dimensional stress field in composite laminates by utilizing 6-node triangular elements relying on multilayer higher-order theory. Romera *et al.* [20] developed a 3-D FE model with solid elements to investigate the free edge effect of angle-ply composite laminates under uniform one-dimensional stretch. They reported that high-stress gradients have appeared at the interface of the laminate close to the free edge regions. In such a problem, a huge number of elements are required to obtain accurate results. Therefore, they employed the sub-modeling technique to increase the nodal density and overcome this problem. Cao *et al.* [2] conducted an experimental program in addition to a 3-D FE model to investigate the complex failure modes of curved composite laminates under a 4-point loading test. The FE model is developed with 0 thickness cohesive elements and based on a mixed-mode traction separation damage law. The results demonstrated that the FE approach is able to predict the stacking sequence failure modes. The free edge effect in the composite laminates was examined by Islam and Prabhaker [1]. For this purpose, they used a FE model with a Quasi-2D plane strain formulation. The results of this examination showed that the computational time is reduced by 30 times when using the Q-2D model, compared to the 3-D analysis of the same laminating. Recently, a scaled boundary FE method merged with a coupled stress and energy failure criterion is employed by Dölling *et al.* [21] to investigate the free edge effect of symmetric angle-ply composite laminates. The model has been validated by comparing its results with the numerical reference solutions which are available in the literature. They reported that the use of this technique can accurately represent the 3-D stress state as well as resolving the stress singularity at the bi-material notch.

This work aims to give more insight into the free edge effect in composite laminates. A better understanding of the physics of delamination failure of cross-ply laminates is a major objective of this research. The cause of delamination that starts at the free edge and propagates towards the interior region has to be addressed clearly based on accurate determination of the stress field, especially in the boundary region. Therefore, delamination failure of such composites can be understood. This research concentrates on solving the problem of accuracy faced by almost all other methods. The accuracy in defining the displacement and stress fields in the vicinity of the free edge and interfaces of laminates can be considered as a major deficiency of many numerical solutions. In addition, the narrow boundary width determination was another drawback in many of those solutions. For most of FE solutions, a huge number of elements are required to obtain accurate results. The main objective of this paper is to overcome the deficiences and drawbacks of other solutions by introducing a numerical FE solution that is capable of attaining accurate results using a small number of elements. To meet above mensioned objectives, the FE modeling is adobted, since geometry and material properties of composites of many laminates can be easily defined and introduced to the FE code. Regions of high stress concentration around holes or edges can be easily detected using different energy and equilibrium theories, different mathematical and numerical methods, different types of elements and number of nodes, and / or different sizing of elements

through mesh generation techniques, etc. Also using special shape functions in the FE model helps in determining accurately displacement and stress fields near the edge even with very narrow boundary width. For this purpose, a 2-D finite element model is developed based on an approximate analytical solution. A perturbation technique is employed to derive shape functions for the free edge boundary region. Galerkin approximation is used to make these shape functions satisfy the governing system of partial differential equations. An original finite element computer program has been written to solve composite laminate problems using 2-dimensional plane strain analysis. It considers one-quarter of the plane and develops algorithms for; special mesh generation and refinement and associated elements and nodes numbering, specific type of shape functions and special numerical integration procedure. It defines element stiffness matrices, performs assemblage, partitioning, applies the required loads and constraints, and performs numerical solutions of system of linear equations. The numerical integration algorithm uses an exact integration of exponential functions in the width direction of the boundary region while Gauss Quadrature integration in other direction and interior region. Interlaminar normal and shear stress distributions for 4 layers of bidirectional laminates with different stacking sequences are investigated for different geometric ratios. Moreover, the effect of mesh refinement on the solution is examined. Results established using the present solution are compared with results of other solutions including the finite difference solution by Pagano [13], the FE solution by Wang and Crossman [16], the perturbation solution by Hsu and Herakovich [10], and the analytical solution by Wang and Dickson [30].

Formulation of the problem

The balanced symmetrical composite laminated plate shown in **Figure 1** is subjected to a constant axial strain, ϵ_0. The order of dimensions is $L_1>L_2>>L_3$. The laminates are homogeneous and orthotropic, and one of the orthotropic axis coincides with X_3-axis. The laminates are of thicknesses ($h_1/ h_2/ h_3/\ldots/ h_m$), and are oriented at angles $(\theta_1/\theta_2/\theta_3/,\ldots/\theta_m)$, with respect to X_1-axis.

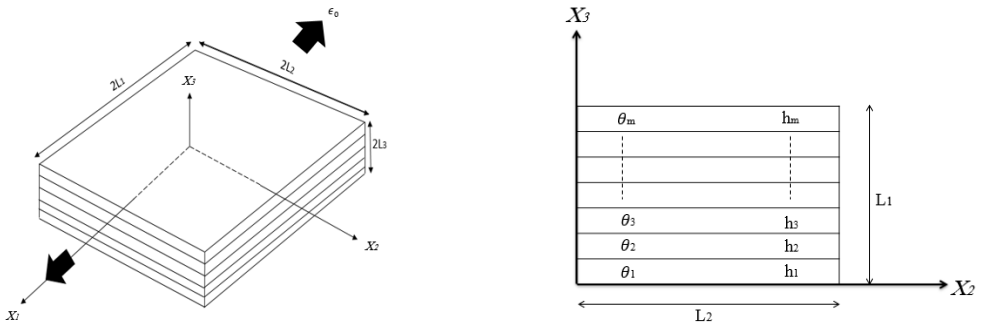

(a) (b)

Figure 1 (a) 2 m composite laminate subjected to a constant axial strain ϵ_0 and (b) X_2-X_3 plane shows different angle orientation and different thicknesses of laminate.

In general, the stress-strain relationship is:

$$\{\sigma\} = [E]\{\epsilon\} \quad (1)$$

where, $\{\sigma\}$ is the stress vector, $\{\epsilon\}$ is the strain vector, and $[E] = E_{ij} \quad i = 1,2,\ldots,6. \; j = 1,2,\ldots,6.$ is the elasticity matrix. For a completely anisotropic material, 21 independent elastic constants are necessary to define the 3-dimensional constitutive equations. The elasticity matrix, in this case, is symmetric and in general, has no 0 terms. For an orthotropic material in which one of the orthotropic axes of laminate coincides with the X_3-axis, the constitutive equations with respect to the coordinate axes X_1, X_2, X_3 are defined as follows:

$$\begin{Bmatrix}\sigma_1\\ \sigma_2\\ \sigma_3\\ \sigma_4\\ \sigma_5\\ \sigma_6\end{Bmatrix} = \begin{bmatrix}E_{11} & E_{12} & E_{13} & 0 & 0 & E_{16}\\ E_{12} & E_{22} & E_{23} & 0 & 0 & E_{26}\\ E_{13} & E_{23} & E_{33} & 0 & 0 & E_{36}\\ 0 & 0 & 0 & E_{44} & E_{45} & 0\\ 0 & 0 & 0 & E_{45} & E_{55} & 0\\ E_{16} & E_{26} & E_{36} & 0 & 0 & E_{66}\end{bmatrix}\begin{Bmatrix}\epsilon_1\\ \epsilon_2\\ \epsilon_3\\ \epsilon_4\\ \epsilon_5\\ \epsilon_6\end{Bmatrix} \quad (2)$$

Only 13 elastic independent constants are necessary to define the 3-dimensional constitutive equations. Because the laminate is considered long and only loaded at its ends $X_1 = \pm L_1$, Saint Venant principle can be invoked, resulting in the conclusion that the stresses in regions far away from the ends are independent of X_1 and $\sigma_{1,1} = \sigma_{5,1} = \sigma_{6,1} = 0$. Thus, the equilibrium equations in such regions are:

$$\begin{aligned}&\sigma_{6,2} + \sigma_{5,3} = 0\\ &\sigma_{2,2} + \sigma_{4,3} = 0\\ &\sigma_{4,2} + \sigma_{3,3} = 0\end{aligned} \quad (3)$$

Using symmetric and anti-symmetric conditions, the following system of simultaneous partial differential equations are obtained for each layer:

$$\begin{aligned}&\{E_{66}\Delta_{1,22} + E_{55}\Delta_{1,33} + E_{26}\Delta_{2,22} + E_{45}\Delta_{2,33} + (E_{36} + E_{45})\Delta_{3,23}\}^{(k)} = 0\\ &\{E_{26}\Delta_{1,22} + E_{45}\Delta_{1,33} + E_{22}\Delta_{2,22} + E_{44}\Delta_{2,33} + (E_{23} + E_{44})\Delta_{3,23}\}^{(k)} = 0\\ &\{(E_{45} + E_{36})\Delta_{1,23} + (E_{44} + E_{23})\Delta_{2,23} + E_{44}\Delta_{3,22} + E_{33}\Delta_{3,33}\}^{(k)} = 0\end{aligned} \quad (4)$$

where $\Delta_1, \Delta_2, \Delta_3$ are displacements in X_1, X_2, X_3 directions and the superscript k denotes the k^{th} layer. The boundary conditions must be satisfied at the free edges $X_2 = \pm L_2$, and also on the top and bottom surfaces of the laminates $X_3 = \pm L_3$.

A section perpendicular to the X_3-axis at the top of the k^{th} layer is analyzed, and only one quarter of the laminate is considered. The free body diagrams above and below this section, as viewed from the X_1-direction, are pictured in **Figure 2**. Equilibrium of forces in the X_2-direction above the section and equilibrium of moments are satisfied. For the free body diagram above the section also as shown in **Figure 3**, equilibrium of forces in the X_1-direction are also satisfied.

A perturbation solution including interior and boundary regions of the displacement in X_2 and X_3 directions is of the following form [7,28]:

$$\begin{aligned}\Delta_2(X_2, X_3) &= A_{21}(X_2)X_3 + A_{22}(X_2) + \left[C_{21}e^{-\lambda_1\alpha(1-X_2)/\epsilon} + C_{22}e^{-\lambda_2\alpha/\epsilon(1-X_2)}\right] cos\alpha X_3\\ \Delta_3(X_2, X_3) &= A_{31}(X_2)X_3 + A_{32}(X_2) + \left[C_{31}e^{-\lambda_1\alpha(1-X_2)/\epsilon} + C_{32}e^{-\lambda_2\alpha/\epsilon(1-X_2)}\right] sin\alpha X_3\end{aligned} \quad (5)$$

where $X_2 = x_2/L_2$, $X_3 = x_3/L3$ and $\epsilon = L_2/L_3$. A_{21}, A_{22}, A_{31}, and A_{32} are functions of X_2 and C_{21}, C_{22}, C_{31}, and C_{32} are constants. α is the common eigenvalue, and

$$E_{00} = \frac{E_{33}}{E_{44}} - \frac{E_{23}E_{23} + 2E_{23}E_{44}}{E_{22}E_{44}}$$

$$\lambda_1 = -\sqrt{\frac{E_{00} + \sqrt{E_{00}^2 - 4\frac{E_{32}}{E_{22}}}}{2}}$$

$$\lambda_2 = -\sqrt{\frac{E_{00} - \sqrt{E_{00}^2 - 4\frac{E_{32}}{E_{22}}}}{2}}$$

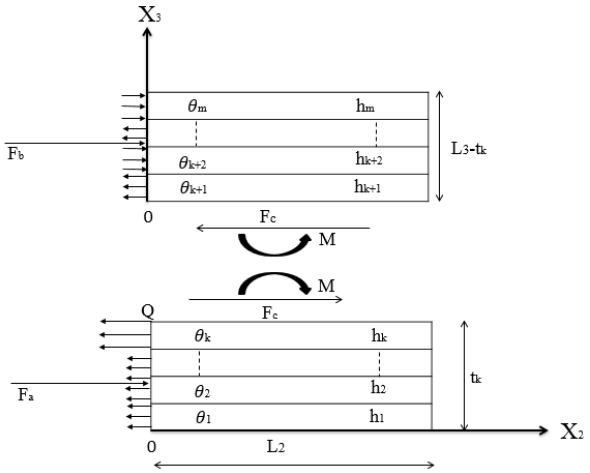

Figure 2 Free body diagram of quarter X_2 - X_3- plane with section at t_k from X_2-axis. Note σ_5, σ_6 are not shown.

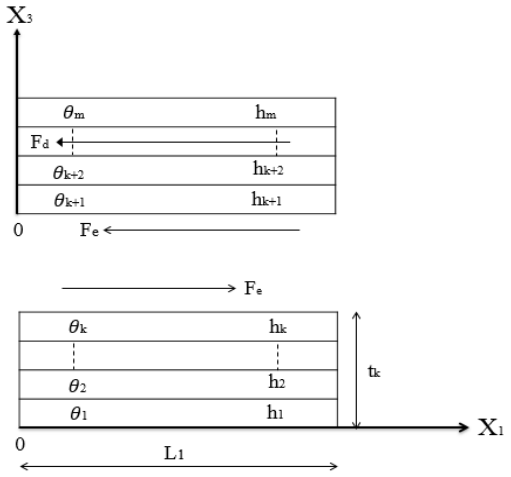

Figure 3 Free body diagram of quarter X_1 X_3 – direction with section at t_k from X_1-axis. Note $\sigma_1, \sigma_2, \sigma_3, \sigma_4$ are not shown.

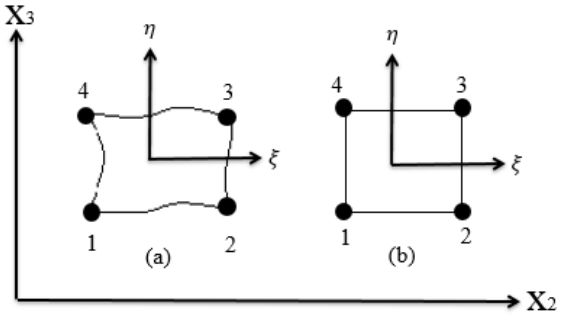

Figure 4 Two-dimensional mapping of 2-D isoparametric (a) curvilinear element and (b) rectangular element.

For bidirectional laminate where the orientation of lamina is 0° or 90° with respect to the X_1-axis, the warping function $\Delta_1(X_2, X_3)$ is 0 and the problem is reduced to a 2-dimensional problem. A 2-dimensional 4 nodes rectangular isoparametric element is used. Standard shape functions are used to define the displacements within the interior region elements, while exponential shape functions are used

to define the displacements within the boundary elements. The isoparametric elements which are shown in **Figure 4** have the following geometric mapping from the global plane (X_2, X_3) to the local plane (ξ, η)

$$X_2 = \sum_{i=4}^{4} \psi_i X_2^{(i)}$$
$$X_3 = \sum_{i=4}^{4} \psi_i X_3^{(i)} \quad (6)$$

where $X_2^{(i)}$, $X_3^{(i)}$ *(i=1,2,3,4)* are the global coordinates of the i^{th} node and ψ_i is the standard 2-D shape function corresponding to the i^{th} node. For interior region elementary the shape functions are:

$$\psi_i = \frac{1}{4}(1 + \xi_i \xi)(1 + \eta_i \eta) \quad (7)$$

where $\xi_i = -1,1,1,-1$ for *i=1,2,3,4* , $\eta_i = -1,-1,1,1$ for *i=1,2,3,4* and ξ, η are the local coordinates. The rigid body mode $\sum_{i=4}^{4} \psi_i$ is satisfied and ψ_i has the value of one at the i^{th} node and 0 at the other nodes.
The 2-D shape functions for the boundary elements are:

$$\mu_{1i} = \alpha_1 \psi_i + (1 - \alpha_1)\phi_{1,i}$$
$$\mu_{2i} = \alpha_2 \psi_i + (1 - \alpha_2)\phi_{2,i} \quad (8)$$

where *i = 1,2,3,4.* μ_{1i}, μ_{2i} define the displacements in the ξ, η directions respectively, $\phi_{1,i}, \phi_{2,i}$ take exponential form and α_1, α_2 are smoothing parameters. ψ_i is the interior region shape functions as defined in Eq. (7). The interior region 0^{th} order perturbation solution, which is the 1^{st} part of the combined solution Eqs. (10), is represented by $\alpha_1 \psi_i, \alpha_2 \psi_i$ in the ξ, η directions, respectively. The 2^{nd} part of Eqs. (8) is represented by $(1 - \alpha_1)\phi_{1,i}$, $(1 - \alpha_2)\phi_{2,i}$ which take care of the exponential growth of the displacements in the ξ - direction and assume linear variation in the η -direction instead of the sine and cosine. For nodes 1,2,3,4 of the boundary element, the shape functions defining the *v*-displacement and *w*-displacement are given in the appendix, where q_{11},q_{12},q_{21},q_{22} are constants.

The shape functions in (A1) and (A2) satisfy the rigid body mode. For the shape functions μ_{1i}, μ_{2i} to have a value of one at i^{th} node and 0 at other nodes, it is required that;

$$q_{11+}q_{12} = 1$$
$$q_{21+}q_{22} = 1 \quad (9)$$

The shape functions of the boundary nodes 2 and 3 are substituted in the governing system of partial differential equations. Then, they are multiplied by a weight function in η and integrated over the boundary ($\xi = 1$) from $\eta = -1$ to $\eta = 1$. Using the Galerkin Weighted Residual Approximation, the linear shape function in η is used as a weighting function. The following functions are derived.

$$\frac{q_{12}}{q_{11}} = -\frac{(\lambda_1/\epsilon)^2 - \lambda_1/\epsilon}{(\lambda_2/\epsilon)^2 - \lambda_2/\epsilon}$$
$$\frac{q_{22}}{q_{21}} = -\frac{(\lambda_1/\epsilon)^2 - \lambda_1/\epsilon}{(\lambda_2/\epsilon)^2 - \lambda_2/\epsilon} \quad (10)$$

Also, α_1, α_2 are defined as follows:

$$\alpha_1 = \frac{\left(1 - 2\frac{\lambda_1}{\epsilon}\right) q_{11} + (1 - 2\frac{\lambda_2}{\epsilon}) q_{12}}{1 - [\left(1 - 2\frac{\lambda_1}{\epsilon}\right) q_{11} + (1 - 2\frac{\lambda_2}{\epsilon}) q_{12}]}$$
$$\alpha_2 = \frac{\left(1 - 2\frac{\lambda_2}{\epsilon}\right) q_{21} + (1 - \frac{\lambda_2}{\epsilon}) q_{22}}{1 - [\left(1 - 2\frac{\lambda_2}{\epsilon}\right) q_{21} + (1 - \frac{\lambda_2}{\epsilon}) q_{22}]} \quad (11)$$

A point (p) within a 2-dimensional isoparametric rectangular finite element, as shown in **Figure 4**, has the following global coordinates in terms of the local coordinates:

$$X_2 = X_{2e} + \frac{H_\xi}{2}\xi$$
$$X_2 = X_{3e} + \frac{H_\eta}{2}\eta \quad (12)$$

where X_{2e}, X_{3e} are the global coordinates of the centroid of the element and H_ξ, H_η are the dimensions of the element in the ξ, η directions respectively. The displacements of the point p are given in terms of the displacements of the 4 corner nodes as follows:

$$v = \sum_{i=4}^{4} N_{1i} v_i$$
$$w = \sum_{i=4}^{4} N_{2i} w_i \quad (13)$$

where $N_{1i} = \psi_{1i}$, $N_{2i} = \psi_{2i}$, for the interior region elements and $N_{1i} = \mu_{1i}$, $N_{2i} = \mu_{2i}$, for the boundary elements. Eqs. (13) could be written in matrix form as follows:

$$\begin{Bmatrix} v \\ w \end{Bmatrix} = [N]\{d\} \quad (14)$$

where

$$[N] = \begin{bmatrix} N_{11} & 0 & N_{12} & 0 & N_{13} & 0 & N_{14} & 0 \\ 0 & N_{21} & 0 & N_{22} & 0 & N_{23} & 0 & N_{24} \end{bmatrix}$$

and

$$\{d\} = [v_1\ w_1\ v_2\ w_2\ v_3\ w_3\ v_4\ w_4]^T$$

Minimization total potential energy yields the following equilibrium equations for each element:

$$[K]\{d\} = \{R\} \quad (15)$$

where

$$[K] = \int_{-1}^{1}\int_{-1}^{1} [B]^T \begin{bmatrix} E_{22} & E_{23} & 0 \\ E_{23} & E_{33} & 0 \\ 0 & 0 & E_{44} \end{bmatrix} [B] d\xi d\eta$$

is the stiffness matrix and

$$\{R\} = -\int_{-1}^{1}\int_{-1}^{1} \epsilon_0 [B]^T \begin{Bmatrix} E_{12} \\ E_{13} \\ 0 \end{Bmatrix} d\xi d\eta$$

is the applied nodal forces in the ξ, η plane due to the constant axial strain in the X_1 direction. Also note that,

[B] = [H][Γ][N']

[Γ] = [$\frac{2}{H_\xi}$ $\frac{2}{H_\eta}$ $\frac{2}{H_\xi}$ $\frac{2}{H_\eta}$] is a 4x4 diagonal matrix,

$$[H] = \begin{bmatrix} 1 & 0 & 0 & 0 \\ 0 & 0 & 0 & 1 \\ 0 & 1 & 1 & 0 \end{bmatrix}$$

And

$$[N'] = \begin{bmatrix} N_{11,\xi} & 0 & N_{12,\xi} & 0 & N_{13,\xi} & 0 & N_{14,\xi} & 0 \\ N_{11,\eta} & 0 & N_{12,\eta} & 0 & N_{13,\eta} & 0 & N_{14,\eta} & 0 \\ 0 & N_{21,\xi} & 0 & N_{22,\xi} & 0 & N_{23,\xi} & 0 & N_{24,\xi} \\ 0 & N_{21,\eta} & 0 & N_{22,\eta} & 0 & N_{23,\eta} & 0 & N_{24,\eta} \end{bmatrix}$$

Results and discussion

Results for special unidirectional [0°, 90°]s, and [90°, 0°]s, graphite-epoxy laminates are presented in this paper. The ply properties of high modulus graphite-epoxy unidirectional composite system are: $E_1 = 20\times10^6$ *psi*, $E_2 = E_3 = 2.1\times10^6$ *psi*, $G_{12} = G_{13} = G_{23} = 0.85\times10^6$ *psi*, and $v_{12} = v_{13} = v_{23} = 0.21$, where *1,2,3* refer to the X_1, X_2, X_3 directions which are the fiber, transverse and the thickness directions, respectively and v_{12} for example is the Poisson's ratio measuring strain in the X_2 direction due to uniaxial tension in the X_1 direction. The stiffness coefficients for both 0° and 90° ply-orientations are listed in **Table 1**. The composite laminates are symmetric, i.e, $\theta(X_3) = \theta(-X_3)$ with constant ply thickness L_0, and constant width $2L_2$. They are subjected to a uniform axial strain $\epsilon_1 = \epsilon_0 = 1 \times 10^{-6}$ in/in in the X_1 direction. This 3-dimensional problem is reduced to 2 dimensional by analyzing the transverse plane (X_2, X_3) through Poisson's ratio. Also, central plane ($X_1 = 0$) is analyzed because it is subjected to maximum transverse displacement fields in X_2 and X_3 in addition to maximum inter-laminar normal stress σ_3 and shear stress σ_4, relative to other transverse planes. Also, due to symmetry one quarter of this transverse plane is analyzed. It is obvious from the physics of the problem that the central point ($X_1 = 0$, $X_2 = 0$ and $X_3 = 0$) has 0 displacement in all 3 perpendicular directions and displacements are increased in positive and negative direction of 3 axes. It also expected that the rate of change of the displacements in transverse directions is rapidly increased at the top and bottom free surfaces and also at free edges. The perturbation solution yields exponential functions that define this rapid increase.

Table 1 Stiffness coefficients for 0° and 90° ply-orientation.

0° ($\times10^6$ psi)	**90° ($\times10^6$ psi)**
$E_{11} = 20.2$	$E_{11} = 2.21$
$E_{12} = 0.56$	$E_{12} = 0.56$
$E_{13} = 0.56$	$E_{13} = 0.48$
$E_{22} = 2.21$	$E_{22} = 20.2$
$E_{23} = 0.48$	$E_{23} = 0.56$
$E_{33} = 2.21$	$E_{33} = 2.21$
$E_{44} = 0.85$	$E_{44} = 0.85$

[0°, 90°]s Bidirectional laminates

Interlaminar stresses in composite laminates have an unusual behavior in the boundary region due to the free-edge effects. **Figures 5** and **6** show the distributions of interlaminar normal stress σ_3 and shear stress σ_4, respectively. As shown in these figures, the boundary layer width decreases as ϵ becomes smaller. Interlaminar normal stress σ_3 increases fast when approaching the free edge. A simple physical explanation of such normal stress distribution is that; normal inter-laminar resultant force acting on 90° layer from 0° layer should vanish to satisfy equilibrium of the 90° layer in X_3 direction. Since small compressive stress is acting on large inter-face area of interior region, therefore, a large tensile stress is needed to act on small interface area of boundary region in tension. Tensile and compressive forces should balance or on other words stress resultant should vanish. A same stress resultant should vanish on the opposite face of 0° layer acting by 90° layer. It should be noted that the stress distribution is the same in the negative X_2 direction because of symmetry. The extreme variability in this stress distribution in the neighborhood (L_2, L_0) serves as strong evidence of possible stress singularity. Singularity is due to the fact that boundary width might be so narrow for even high tensile stress and therefore tensile stress resultant can balance compressive force. Hence, singularity is a strong evidence of possible delamination that is initiated locally at the vicinity of the point (L_0, L_2). Delamination continues to propagate in the perpendicular X_0 and X_2 directions until global failure. Singularity is believed to be a result of the discontinuity in elastic properties at the interface between the 0° and 90° layers. The normal stress σ_3

converge to finite values at the exact free edge for different geometric ratios. These values are slightly less for smaller ϵ, simply because the compressive stress is also slightly less for smaller ϵ. The distributions of the interlaminar stresses in the interior region indicate an asymptotic recovery of the lamination theory. Interlaminar shear stress σ_4 can cause shearing delamination since its magnitude close to the free edge might be large enough. **Figure 6** shows that this shear stress has a negative value for the specified stack sequence in the positive X_2 direction. Equilibrium of forces in the X_2 direction is satisfied as the shear stress resultant is balanced by the normal stress, (σ_2) resultant along axis X_3. The shear stress distribution is the same in the negative X_2 direction, but with opposite positive sign. The magnitude of this stress increases fast while approaching the boundary but goes back to 0 at the exact free edge. This is required by the stress-free boundary condition at the exact free edge. It should be noted here that whether the exact elasticity solution satisfies that the traction-free boundary condition is not known. The maximum negative value of σ_4 does not vary much for different geometric ratios ϵ and it is slightly less for smaller ϵ. It does not vary much because of 2 main reasons. First, it has to adjust in a small boundary region to be 0 at the exact free edge, and second, the normal stress (σ_2) along the axis X_3 does not vary much for different ϵ. Moment equilibrium equation is also satisfied for quarter plane and for any layer within this plane. **Figure 7** shows the normal stress distributions in the boundary region for small geometric ratios. This stress is evaluated at the interface $X_3 = L_0$; taking the 90° as a reference layer. It is shown in this figure that the distribution of stress is smooth and continuous. The size of the boundary layer width is shown clearly for small geometric ratios. Similarly, **Figure 8** shows the shear stress distribution for small geometric ratios. It is shown in this figure that the peak value of shear stress does not vary much for different values of ϵ.

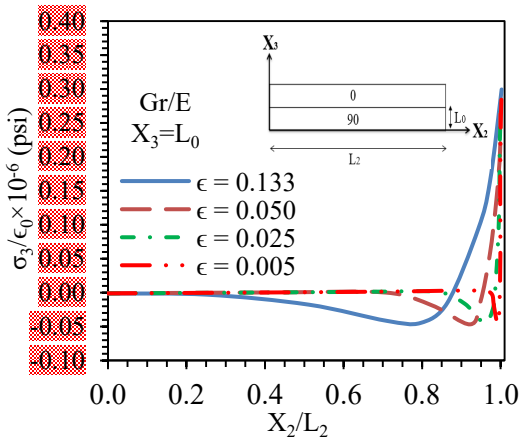

Figure 5 Interlaminar normal stress σ_3 at $X_3 = L_0$ for different values of ϵ for $[0/90]_s$.

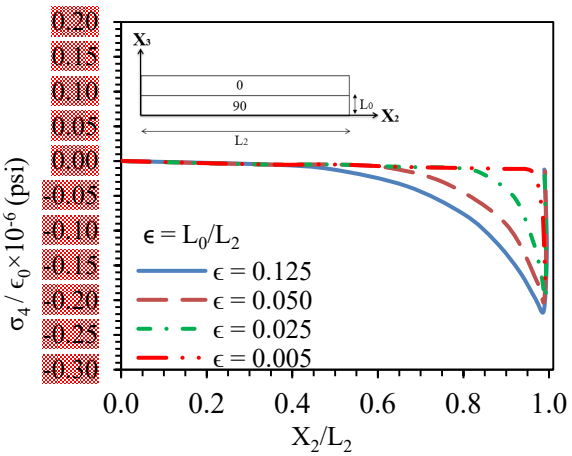

Figure 6 Interlaminar shear stress σ_4 in the 90° layer at the interface $X_3 = L_0$ for different geometric ratios.

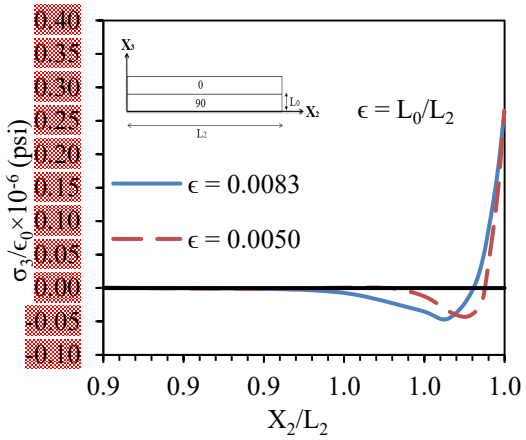

Figure 7 Interlaminar normal stress σ_3 for small geometric ratios in the boundary region of 90° layer at the interface $X_3 = L_0$.

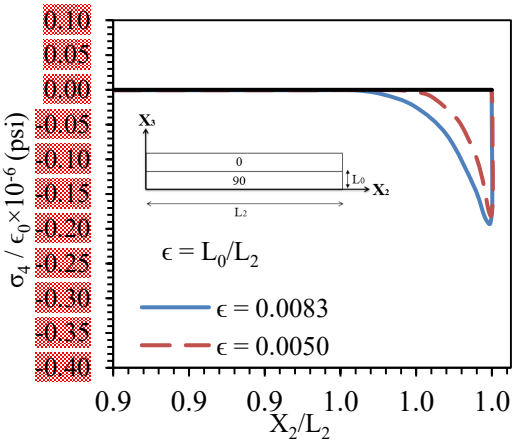

Figure 8 Interlaminar shear stress σ4 in the boundary region of the 90° layer at the interface $X_3 = L_0$ for very small geometric ratios.

Comparative results for the distribution of the displacement δ_2 in the width direction at the free surface $X_3 = 2L_0$ are shown in **Figure 9**. It is shown in this figure that the variation of this displacement is almost the same using the specified different approaches. In the interior region, this displacement filed is almost liner and no differences are noticed between the differently solution procedures. Therefore, this suggests that all different solutions provide an asymptotic recovery of the classical lamination theory in the interior region. **Figure 10** shows the distribution of the normal stress σ_3 along the width direction of the central plane $X_3 = 0$ for a large geometric ratio, $\epsilon = 0.125$. It is shown in this figure that the different solution procedures agree very well, especially the present solution and solution by Pagano [13]. The present solution yields a slightly smaller boundary layer width than the other solutions [13,16]. **Figures 11** and **Figure 12** show σ_3 and σ_4 respectively at the [0°, 90°]s interface, $X_3 = L_0$ for $\epsilon = 0.125$. It is clear that the present solution agrees very well with Pagano's [13] solution. The finite element solution by Wang and Crossman [16] gives lower values of the normal stress at the exact free edge and the peak shear stress. This is because their solution procedure is too dependent on the element's sizes in the free edge region. A very refined mesh is needed to establish accurate results using the solution procedure in [16]. A uniform mesh of 80 4-nodes rectangular elements are used to establish the results of the present solution which are shown in **Figures 9 - 12**. Wang and Crossman [16] used a non-uniform mesh of 576 triangular elements to come up with their results which are shown in the same figure. This suggests that the present approach is superior to the finite element procedure [16] in saving computer storage and computing time. It is hard to establish an accurate solution using Pagano's theory [13] or the method by Wang and Crossman [16] for laminates consisting of very many layers. The reason is that too many elements are

needed, which yields to unreasonable computer storage and computing time. Moreover, using the methods proposed by these authors will not yield satisfactory results for laminates with small geometric ratios. However, the present method is applicable for laminates consisting of too many layers and produces accurate results for laminates with small geometric ratios, because only a few elements are needed for each layer. For geometric ratio $\epsilon = 0.025$, the distribution of normal stress σ_3 evaluated in the present work is compared to those evaluated by the perturbation solution [10], and the solution by Wang and Dickson [30] as shown in **Figure 13**. There is a good agreement between the present solution and the solution by Wang and Dickson [30] for small geometric ratios. However, their solution gives higher values of stress at the exact free edge for small geometric ratios. As shown in **Figure 13**, the perturbation solution [10] yields a very small boundary layer width and a low normal stress value at the free edge. The reason is that the accuracy of the perturbation solution depends mainly on the geometric ratio and the relative values of material constants. It should be noted here that the distribution of normal stress is established using the 90° layer as a reference layer. The perturbation solution [10] is not expected to give a good accuracy when using the 90° layer as reference layer. This is due to the relative values of material constants, as illustrated in the following: The coupled governing system of partial differential equations for bidirectional laminates is:

$$\begin{aligned}&(\frac{L_3}{L_2})^2 E_{22}\Delta_{2,22} + E_{44}\Delta_{2,33} + \left(\frac{L_3}{L_2}\right)(E_{44}+E_{23})\Delta_{3,23} = 0\\ &(\frac{L_3}{L_2})(E_{44}+E_{23})\Delta_{2,23} + (\frac{L_3}{L_2})^2 E_{44}\Delta_{3,22} + E_{33}\Delta_{3,33} = 0\end{aligned} \tag{16}$$

which for $L_2/L_3 = 0.05$ becomes:

$$(0°)\begin{cases}0.0065\Delta_{2,22} + \Delta_{2,33} + 0.0782\,\Delta_{3,23} = 0\\ 0.030\Delta_{2,23} + 0.001\,\Delta_{3,22} + \Delta_{3,33} = 0\end{cases} \tag{17}$$

$$(90°)\begin{cases}0.05\Delta_{2,22} + \Delta_{2,33} + 0.083\,\Delta_{3,23} = 0\\ 0.032\Delta_{2,23} + 0.001\,\Delta_{3,22} + \Delta_{3,33} = 0\end{cases} \tag{18}$$

It can be observed from Eqs. (17) and (18) that a perturbation solution using the 0° layer as a reference layer should lead to more accurate results. Moreover, the 0th order perturbation solution is improved by diminishing ϵ.

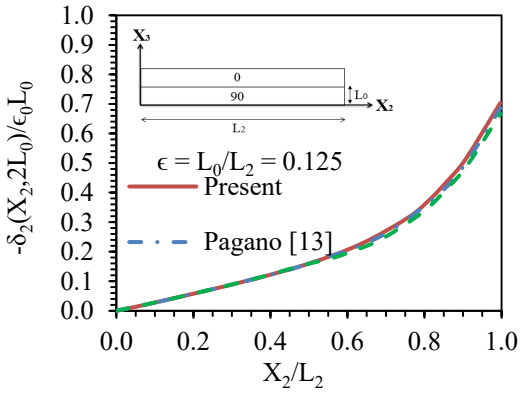

Figure 9 Transverse displacement across the top free surface $X_3 = 2L_0$.

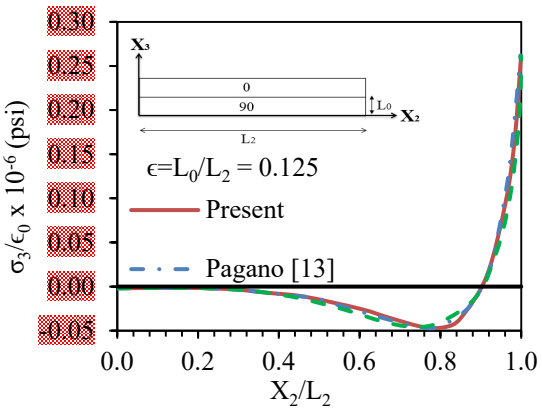

Figure 10 Interlaminar normal stress σ_3 distribution along the width at the central plane $X_3 = 0$.

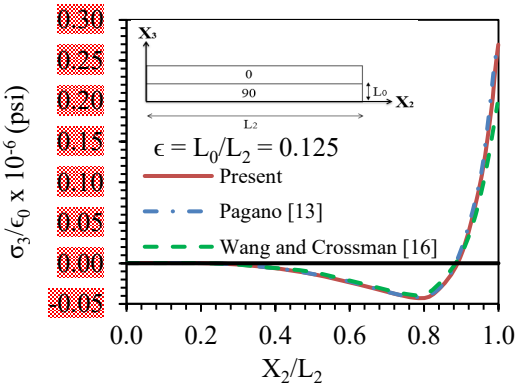

Figure 11 Different results for interlaminar normal stress σ_3 at the interface $X_3 = L_0$.

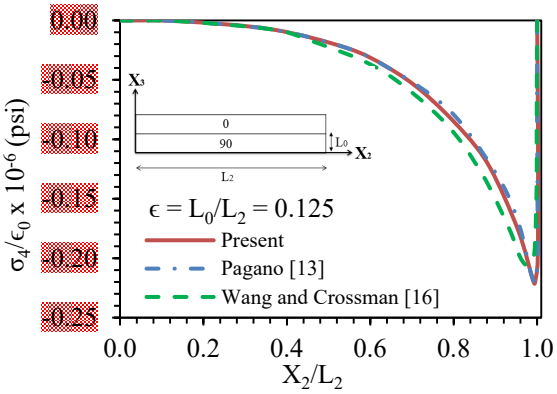

Figure 12 Present, Pagano [13], and finite element [16] results for interlaminar shear stress.

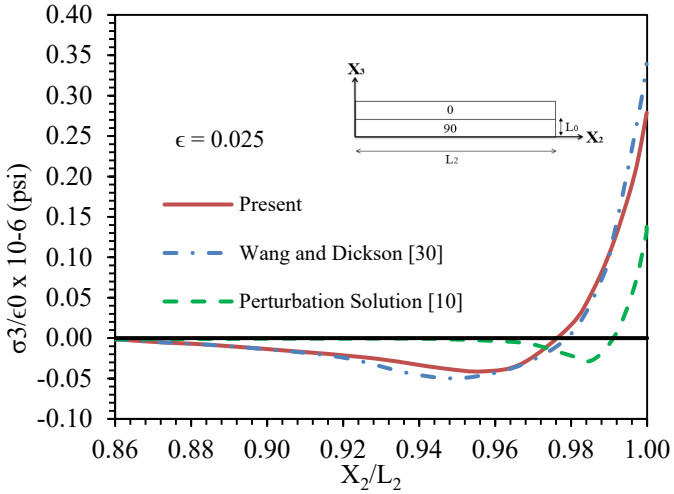

Figure 13 Present, and other results for the normal stress σ_3 in the 90° layer at the interface in the 90° layer at the interface $X_2 = L_0$ for laminates with intermediate geometric ratio ϵ.

[90°, 0°]s Bidirectional laminates

The behavior of the bidirectional laminates for [90°, 0°]s stacking sequence is discussed in this section. It is observed that these laminates behave fundamentally differently than [0°, 90°]s laminates. This is because of a noticeable difference in the magnitude of stresses as X_2/L_2 approaches 1. As expected, σ_3 for [0°, 90°]s and σ_3 for [90°, 0°]s have their sign reversed. As shown in **Figure 14** the normal stress σ_3 converges to a finite maximum negative value at the free edge for different geometric ratios. The magnitude of the normal stress at the exact free edge for the [90°, 0°]s stacking sequence is higher than that of the [0°, 90°]s case. For $\epsilon = 0.125$, the value of σ_3 at the free edge is about 0.25×10^6 psi and -0.37×10^6 psi for [0°, 90°]s and [90°, 0°]s, respectively. Therefore, the [0°, 90°]s laminates are stronger than the [90^0,0^0]s laminates as far as the delamination failure is concerned. In the case of [0°, 90°]s, the middle 2 layers are at 90° and the modulus of elasticity in this transverse direction, $E_{22} = 20.2\times10^6$ psi, while for [90°, 0°]s the middle 2 layers are at 0° and the modulus of elasticity in this transverse direction, $E_{22} = 2.21\times10^6$ psi. Therefore, the middle 2 layers have better resistance to transverse displacement in the X_2 direction while for the case of [90°, 0°]s the 90° layers are the top and bottom layers where the top and bottom faces are free. Hence this stacking sequence should have less resistance capacity. The maximum shear stress value for the [90°, 0°]s laminates is slightly higher than that of [0°, 90°]s laminates as shown in **Figure 14**. Again, for the [90°,0°]s stacking sequence the boundary layer width decreases as the geometric ratio decreases, as shown in **Figures 14 - 16** shows the distribution of normal stress along the width direction for different geometric ratios using the 90° layer as a reference layer. Even though the stresses are evaluated at the same position $X_3 = L_0$, they are different from those using the 0° layer as a reference layer. Thus, discontinuity of stresses at the interface is due to the difference in elasticity coefficients which are dependent on the orientation of each layer. The maximum negative value of the normal stress occurs very close to the boundary and not at the exact free edge. Peak stress is closer to the free edge for smaller ϵ. The values of stress at the free edge and the maximum positive and the maximum negative values of stress are slightly different for different ϵ. It is shown in **Figure 16** that the maximum positive value of normal stress is higher for smaller ϵ and the maximum negative value is lower for smaller ϵ. Again, the boundary layer width is directly proportional to ϵ. Interlaminar shear stresses along the interface $X_3 = L_0$ for [90°/0°/0°/90°] laminate are plotted in **Figure 17**. This figure shows the distribution of shear stress in the boundary region for intermediate and small geometric ratios. In order to determine clearly the variation of shear stress near the free edge, more elements are used in this region. Although the positive peak stress is almost the same for different ϵ, the smaller ϵ is the sharper peak stress and its closer to the free edge. Results for interlaminar normal stress σ_3 along the centerline $X_3 = 0$ using the present approach is plotted in **Figure 18** and compared with existing results by Wang and Crossman [16]. Even though σ_3 from both solutions converge to almost the same finite negative maximum value at the free edge, the present solution provides a smaller boundary layer width and a sharper rise in the magnitude of stress at the free edge. The maximum positive stress is slightly lower for the present

solution approach. As for the [0°/90°/90°/0°] stacking sequence, both solution procedures agree very well in the interior region. The present approach has an advantage over the other finite element approach by Wang and Crossman [16] since considerably less number of elements is needed to establish an accurate solution. The present solution exhibits better agreement with the perturbation solution [10] for the [90°/0°/0°/90°] laminates as shown in **Figure 19**. The value of σ_3 at the exact free edge and the value of maximum positive stress for both solutions approaches are almost the same. The perturbation solution yields more accurate results when using the 0° as a reference layer, as illustrated in Eqs. (17) and (18). Since both solutions agree well when using 0° as a reference layer, the displacement between the 2 solutions using 90° as a reference layer, **Figure 13** is believed to be due to a considerable amount of error in the perturbation solution. Therefore, the present solution is more reliable when using the 90° as a reference layer.

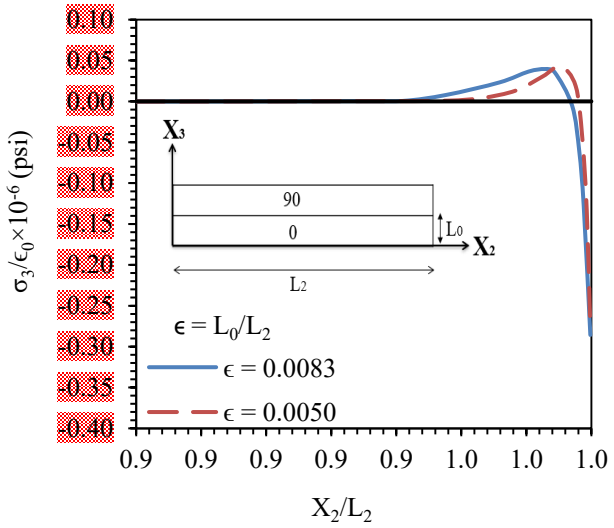

Figure 14 Interlaminar normal stress σ_3 in the 0° layer at the interface $X_3 = L_0$ for small ϵ.

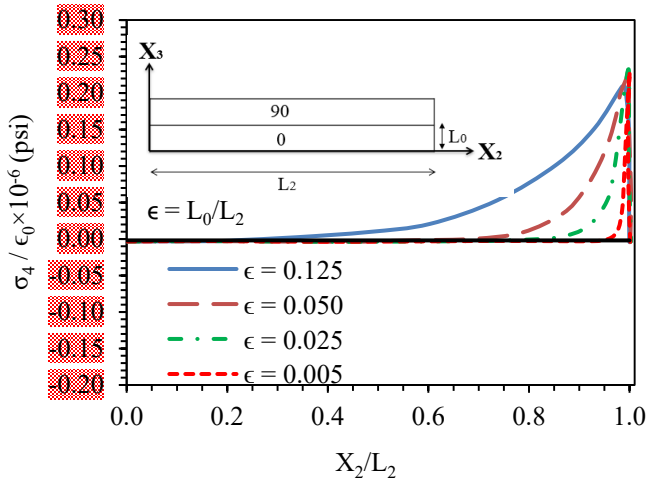

Figure 15 Interlaminar shear stress σ_4 in the 0° layer at the interface $X_3 = L_0$ for different ϵ.

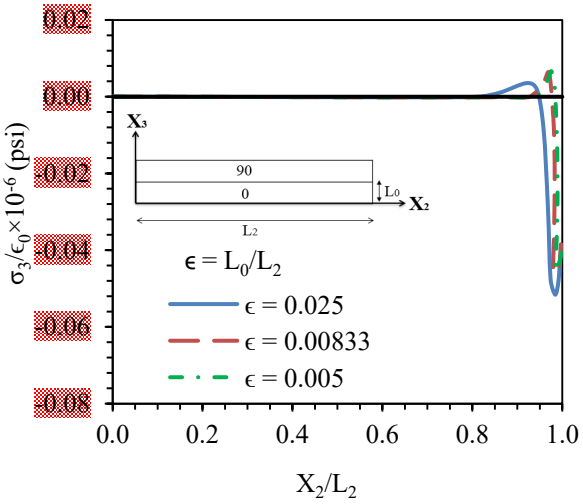

Figure 16 Interlaminar normal stress σ_3 in the 900 layer at the interface $X_3 = L_0$ for different ϵ.

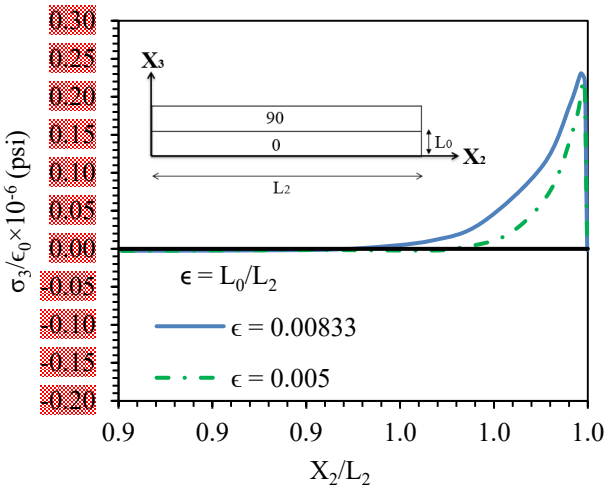

Figure 17 Interlaminar shear stress σ_4 in the boundary region of the 0° layer at the interface $X_3 = L_0$, for small ϵ.

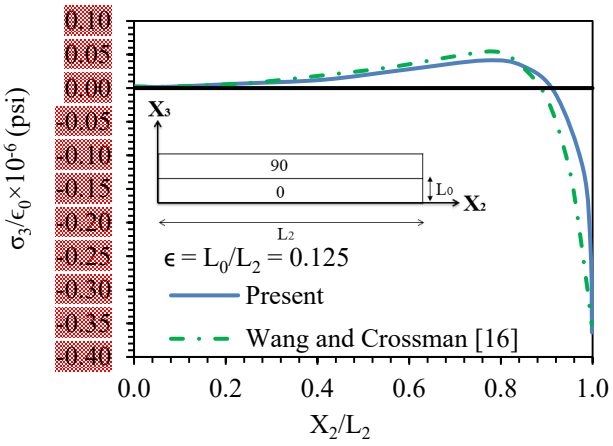

Figure 18 Present and finite element [16] results for interlaminar normal stress σ_3 along the center line $X_3 = 0$.

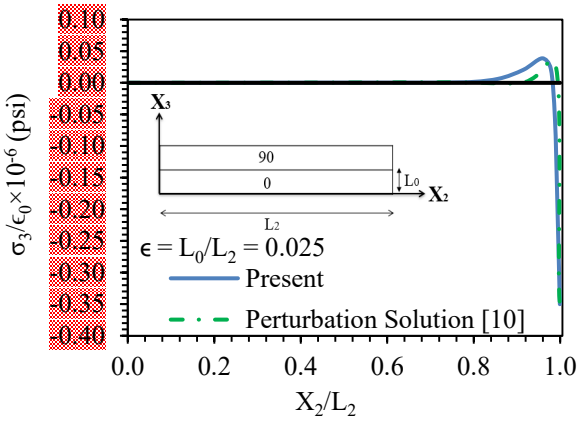

Figure 19 Interlaminar normal stress σ_3 distribution in the 0° layer at the interface $X_3 = L_0$ for

Effect of mesh refinement on the results

Figure 20 shows the distribution of normal stress for a large geometric ratio $\epsilon = 0.0125$ using 10, 20, and 32 elements per layer. The results agree very well in the interior region for the 3 different meshes. Using the uniform mesh of 10 or 20 elements per layer does not yield a clear determination of the stress in the boundary region, and results in a low value of stress at the free edge. The results established using a uniform mesh of 80 elements provide excellent agreement with results from other numerical solutions as shown in **Figures 10 - 12**. Therefore, a coarse mesh is sufficient when using the present solution approach for laminates with large ϵ. As shown in **Figure 21** the distribution of σ_3 using a uniform mesh of 50 elements per layer is compared to that using a non-uniform mesh of the same number of elements of $\epsilon = 0.025$. A non-uniform mesh of 50 elements per layer means that there are 25 elements per layer in the region $0 < X_2/L_2 \leq 0.8$ and 25 elements per layer in the region $0.8 < X_2/L_2 \leq 1$. A refined mesh is not necessary for laminates with an intermediate geometric ratio since using a fine mesh does not improve the results, not to mention the slight improvement of the value of stress at the exact free edge. A uniform and non-uniform meshes of 60 elements per layer are used to estimate the normal stress distribution for the laminate with $\epsilon = 0.00833$ as shown in **Figure 22**. It is obvious that the fine non-uniform mesh yields a smooth and continuous distribution of stress in the boundary region. It provides a clear determination of the positive peak stress and improves the value of stress at the exact free edge. Therefore, a fine mesh in the boundary region is needed only when encountering laminates with small geometric ratios.

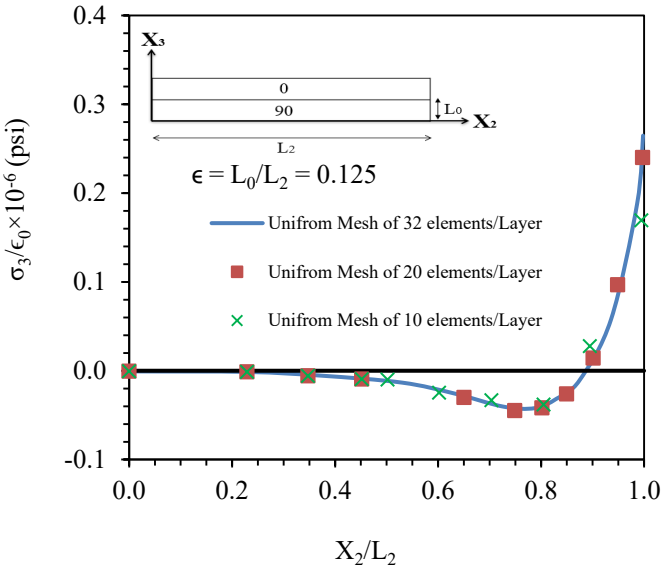

Figure 20 Interlaminar normal stress for $\epsilon = 0.125$ using a uniform mesh of 10, 20 and 32.

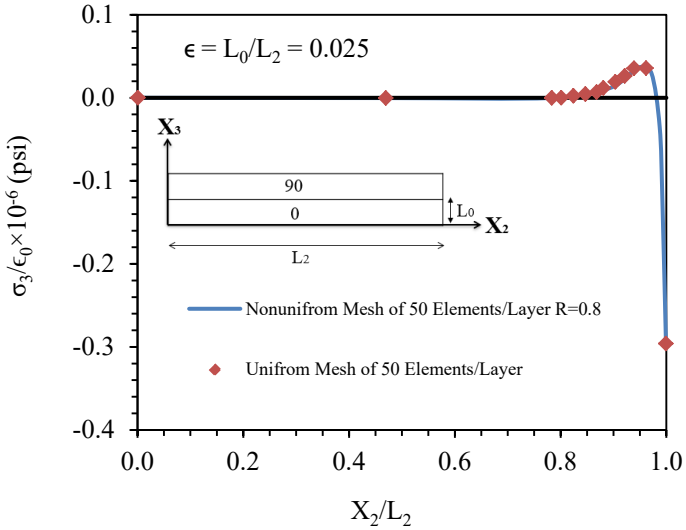

Figure 21 Effect of mesh refinement on the normal stress distribution for $\epsilon = 0.025$.

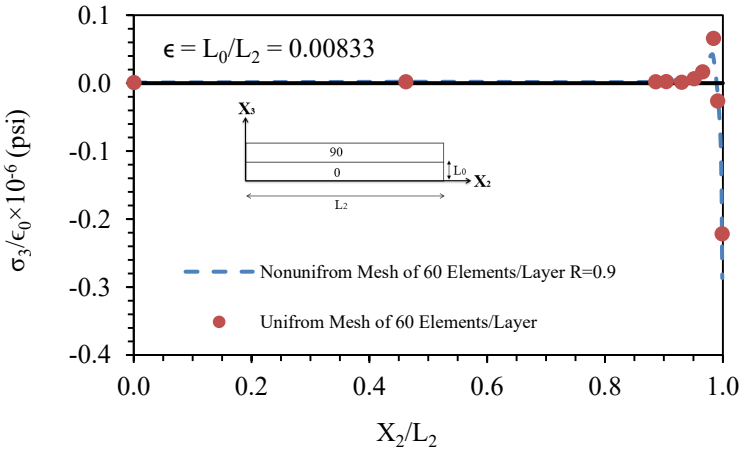

Figure 22 Effect of mesh refinement on the normal stress distribution for $\epsilon = 0.00833$.

Conclusions

A 2-dimensional FE modeling and programing is developed in this paper to have a better insight of edge effect and delamination failure of cross-ply laminates subjected to uniaxial strain. Perturbation solution is used to define special exponential shape functions that satisfy the governing system of partial differential equations in the approximate sense. The proposed FE solution resolves the difficulties involved in previous numerical and approximate analytical approaches for the stress analysis of laminated composites. Among these difficulties are the ones associated with attempts to realistically and accurately define the stress fields and boundary layers in laminates consisting of very many layers or laminates with very small geometric ratio. Another major difficulty is the mathematical complexity associated with this class of boundary value problems. Accurate determination of displacement and stress fields helps in understanding the physical behavior of laminated composites. Specifically, edge effect phenomena and local delamination that propagates in the X_1 and X_2 directions to cause global failure is discussed. It is observed that a high gradient displacement and normal stress fields exist near the free edge. Also, high gradient shear stress field exists near the free edge which decay to recover the classical lamination theory in the interior region. The boundary layer width is directly proportional to the geometric ratio of the laminate. The value of normal stress σ_3 at the exact free edge is finite and does not vary much for different geometric ratios, $0 < \epsilon << 1$. The normal stress σ_3 and the shear stress σ_4 in $[0^0, 90^0]_s$ laminate have their sings reversed in $[90^0, 0^0]_s$ laminate. Therefore, these 2 laminates are believed to behave fundamentally differently since there exist noticeable differences in the magnitudes of stresses for $[0^0,$

$90^0]_s$ and $[90^0, 0^0]_s$ laminates. The $[0^0, 90^0]_s$ stacking sequence has better resistance to axial extension than the $[90^0, 0^0]_s$ one. Singularity appears to be confined to the vicinity of (L_2, L_0) due to the discontinuity in elastic properties and the resulting extreme capability of the displacement and stress fields in this neighborhood. Using the present approach, a fine mesh in the boundary region is only needed for laminates with small geometric ratios. For laminates with large and intermediate geometric ratios, a coarse mesh is sufficient to produce accurate results. This capability of the present solution approach in addition to using the skyline storage scheme makes the solution procedure extremely efficient.

References

[1] M Islam and P Prabhakar. Modeling framework for free edge effects in laminates under thermo-mechanical loading. *Compos. B. Eng.* 2017; **116**, 89-98.

[2] D Cao, H Hu, Q Duan, P Song and S Li. Experimental and three-dimensional numerical investigation of matrix cracking and delamination interaction with edge effect of curved composite laminates. *Compos. Struct.* 2019; **225**, 111154.

[3] JJ Espadas-Escalante, NPV Dijk and P Isaksson. The effect of free-edges and layer shifting on intralaminar and interlaminar stresses in woven composites. *Compos. Struct.* 2018; **185**, 212-20.

[4] D Zhang, J Ye and HY Sheng. Free-edge and ply cracking effect in cross-ply laminated composites under uniform extension and thermal loading. *Compos. Struct.* 2006; **76**, 314-25.

[5] P Lecomte-Grosbras, B Paluch and M Brieu. Characterization of free edge effects: influence of mechanical properties, microstructure and structure effects. *J. Compos. Mater.* 2013; **47**, 2823-34.

[6] T Lorriot, H Wargnier, J Wahl, A Proust and L Lagunegrand. An experimental criterion to detect onset of delamination in real time. *J. Compos. Mater*. 2014; **48**, 2175-89.

[7] P Lecomte-Grosbras, J Réthoré, N Limodin, JF Witz and M Brieu. Three-dimensional investigation of free-edge effects in laminate composites using x-ray tomography and digital volume correlation. *Exp. Mech.* 2015; **55**, 301-11.

[8] DW Oplinger, BS Parker and FP Chiang. Edge-effect studies in fiber-reinforced laminates. Experimental Mechanics. 1974; **14**, 347-54.

[9] CT Herakovich, D Post, MB Buczek and R Czarnek. Free edge strain concentrations in real composite laminates: Experimental-theoretical correlation. *J. Appl. Mech.* 1985; **52**, 787-93.

[10] P Hsu and C Herakovich. *A perturbation solution for interlaminar stresses in bidirectional laminates. In:* J David (Ed.). Composite materials: Testing and design (fourth conference). American Society for Testing and Materials, Pennsylvania, USA, 1977, p. 526.

[11] RB Pipes and NJ Pagano. Interlaminar stresses in composite laminates under uniform axial extension. *J. Compos. Mater.* 1970; **4**, 538-48.

[12] A Solis, S Sánchez-Sáez and E Barbero. Influence of ply orientation on free-edge effects in laminates subjected to in-plane loads. *Compos. B. Eng.* 2018; **153**, 149-58.

[13] N Pagano. Stress fields in composite laminates. *Int. J. Solids Struct.* 1978; **14**, 385-400.

[14] G Isakson A and Levy. Finite-element analysis of interlaminar shear in fibrous composites. *J. Compos. Mater.* 1971; **5**, 273-6.

[15] E Stanton, L Crain and T Neu. A parametric cubic modelling system for general solids of composite material. *Int. J. Numer. Methods Eng.* 1977; **11**, 653-70.

[16] A Wang and FW Crossman. Some new results on edge effect in symmetric composite laminates. *J. Compos. Mater.* 1977; **11**, 92-106.

[17] A Wang and FW Crossman. Calculation of edge stresses in multi-layer laminates by sub-structuring. *J. Compos. Mater.* 1978; **12**, 76-83.

[18] P Bar-Yoseph and J Avrashi. New variational-asymptotic formulations for interlaminar stress analysis in laminated plates. *Z. Angew. Math. Phys.* 1986; **37**, 305-21.

[19] R Barboni, R Carbonaro and P Gaudenzi. On the use of a multilayer higher-order theory for the stress analysis around a circular hole of laminates under tension. *Compos. Struct.* 1995; **32**, 649-58.

[20] JM Romera, MA Cantera, I Adarraga and F Mujika. Application of the submodeling technique to the analysis of the edge effects of composite laminates. *J. Reinf. Plast. Compos*. 2013; **32**, 1099-11.

[21] S Dölling, J Hahn, J Felger, S Bremm and W Becker. A scaled boundary finite element method model for interlaminar failure in composite laminates. *Compos. Struct.* 2020; **241**, 111865.

[22] CR Cater, X Xiao, RK Goldberg and X Gong. The influence of interlaminar microstructure on micro-cracking at laminate free edge. *Compos. A: Appl. Sci. Manuf.* 2018; **110**, 217-26.

[23] B Mohammadi and D Salimi-Majd. Investigation of delamination and damage due to free edge effects in composite laminates using cohesive interface elements. *Eng. Solid Mech.* 2014; **2**, 101-18.

[24] XX Li, D Tian and JH He. High energy surface as a receptor in electrospinning: A good switch for hydrophobicity to hydrophilicity. *Therm. Sci.* 2021; **25**, 2205-12.
[25] X Yao and JH He. On fabrication of nanoscale non-smooth fibers with high geometric potential and nanoparticle's non-linear vibration. *Therm. Sci.* 2020; **24**, 2491-7.
[26] NB Peng and JH He. Insight into the wetting property of a nanofiber membrane by the geometrical potential. *Recent Pat. Nanotechnol.* 2020; **14**, 64-70.
[27] JH He. Seeing with a single scale is always unbelieving: From magic to two-scale fractal. *Therm. Sci.* 2021; **25**, 1217-9.
[28] X Li, Y Li, Y Li and J He. Gecko-like adhesion in the electrospinning process. *Results Phys.* 2020; **16**, 102899.
[29] JD Whitcomb and I Raju. Superposition method for analysis of free-edge stresses. *J. Compos. Mater.* 1983; **17**, 492-507.
[30] JT Wang and JN Dickson. Interlaminar stresses in symmetric composite laminates. *J. Compos. Mater.* 1978; **12**, 390-402.

Appendices

$$\begin{aligned}
\mu_{11} &= \alpha_1[\frac{1}{4}(1-\xi)(1-\eta)] + (1-\alpha_1)[\frac{1}{2}\{1-\frac{1}{2}(1+\xi)(q_{11}e^{\frac{\lambda_1(1-\xi)}{e}} + q_{12}e^{\frac{\lambda_2(1-\xi)}{e}})\}(1-\eta)] \\
\mu_{12} &= \alpha_1[\frac{1}{4}(1+\xi)(1-\eta)] + (1-\alpha_1)[\frac{1}{4}\{(1+\xi)(q_{11}e^{\frac{\lambda_1(1-\xi)}{e}} + q_{12}e^{\frac{\lambda_2(1-\xi)}{e}})\}(1-\eta)] \\
\mu_{13} &= \alpha_1[\frac{1}{4}(1+\xi)(1+\eta)] + (1-\alpha_1)[\frac{1}{4}\{(1+\xi)(q_{11}e^{\frac{\lambda_1(1-\xi)}{e}} + q_{12}e^{\frac{\lambda_2(1-\xi)}{e}})\}(1+\eta)] \\
\mu_{14} &= \alpha_1[\frac{1}{4}(1-\xi)(1-\eta)] + (1-\alpha_1)[\frac{1}{2}\{1-\frac{1}{2}(1+\xi)(q_{11}e^{\frac{\lambda_1(1-\xi)}{e}} + q_{12}e^{\frac{\lambda_2(1-\xi)}{e}})\}(1+\eta)]
\end{aligned} \tag{A1}$$

$$\begin{aligned}
\mu_{21} &= \alpha_2[\frac{1}{4}(1-\xi)(1-\eta)] + (1-\alpha_2)[\frac{1}{2}\{1-\frac{1}{2}(1+\xi)(q_{21}e^{\frac{\lambda_1(1-\xi)}{e}} + q_{22}e^{\frac{\lambda_2(1-\xi)}{e}})\}(1-\eta)] \\
\mu_{22} &= \alpha_2[\frac{1}{4}(1+\xi)(1-\eta)] + (1-\alpha_2)[\frac{1}{4}\{(1+\xi)(q_{21}e^{\frac{\lambda_1(1-\xi)}{e}} + q_{22}e^{\frac{\lambda_2(1-\xi)}{e}})\}(1-\eta)] \\
\mu_{23} &= \alpha_2[\frac{1}{4}(1+\xi)(1+\eta)] + (1-\alpha_2)[\frac{1}{4}\{(1+\xi)(q_{21}e^{\frac{\lambda_1(1-\xi)}{e}} + q_{22}e^{\frac{\lambda_2(1-\xi)}{e}})\}(1+\eta)] \\
\mu_{24} &= \alpha_2[\frac{1}{4}(1-\xi)(1+\eta)] + (1-\alpha_2)[\frac{1}{2}\{1-\frac{1}{2}(1+\xi)(q_{21}e^{\frac{\lambda_1(1-\xi)}{e}} + q_{22}e^{\frac{\lambda_2(1-\xi)}{e}})\}(1+\eta)]
\end{aligned} \tag{A2}$$